Journal of Inorganic and General Chemistry
ZAAC
Zeitschrift für anorganische und allgemeine Chemie
DOI: 10.1002/zaac.202000460
ARTICLE

Cytotoxic Activities of Bis-cyclometalated Rhodium(III) and Iridium(III) Complexes Containing 2,2′-Biphenyldiamine

Marion Graf,[a] Hans-Christian Böttcher,*[a] Nils Metzler-Nolte,[b] Karlheinz Sünkel,[a] Sugina Thavalingam,[b] and Rafał Czerwieniec[c]

Dedicated to Professor Christoph Janiak on the Occasion of His 60th Birthday

The synthesis and characterization of new bis-cyclometalated complex salts $[M(ptpy)_2(2,2'\text{-biphenyldiamine})]PF_6$ (M = Rh, **1**; M = Ir, **2**; ptpy = 2-(*p*-tolyl)pyridinato) are described. Compounds **1** and **2** were obtained by bridge-splitting reactions of $[\{M(\mu\text{-}Cl)(ptpy)_2\}_2]$ (M = Rh or Ir) with 2,2′-biphenyldiamine in CH_2Cl_2/MeOH/H_2O mixtures. The molecular structure of compound **2** in the crystal was confirmed by single-crystal X-ray diffraction. **2** crystallized from dichloromethane/methanol/*n*-heptane in the monoclinic space group $P2_1/_n$. The cytotoxic activities of both new compounds were examined and evaluated. Compound **1** and **2** exhibit significant cytotoxicity against human cancer cell lines with the IC_{50} values in the low micromolar range.

Introduction

Currently metal complexes are in the focus of modern medicinal inorganic chemistry approaches to discover and develop new pharmaceutical metallodrugs.[1] Amongst these compounds of potential candidates in this field, especially iridium(III) complexes containing cyclometalated phenylpyridinato ligands play an important role in studies devoted towards therapy of cancers due to their high cytotoxic activities.[2] Moreover it was shown that modifications of the cyclometalating as well as the ancillary ligands allowed a fine-tuning of the anticancer and imaging properties respectively.[3] In the course of such investigations we were interested in studies of the cytotoxic activity of related compounds towards some human cancer cell lines whereas we included – beside iridium(III) – even bis-cyclometalated rhodium(III) complexes with substituted 2,2-bipyridines or 1,10-phenanthrolines as the ancillary ligands.[4] In this paper we describe the synthesis and the characterization of two new cyclometalated metal(III) compounds of the type $[M(ptpy)_2(L_2)]PF_6$ (M = Rh, **1**; M = Ir, **2**) containing the not yet investigated chelating ancillary ligand L_2 = 2,2′-biphenyldiamine. Furthermore, we demonstrated the potent in vitro antiproliferative activity of the novel compounds **1** and **2**.

Results and discussion

For the synthesis of the cationic mononuclear title complexes we used a bridge-splitting reaction starting from the dimeric precursor compound $[\{M(\mu\text{-}Cl)(ptpy)_2\}_2]$ (ptpy = 2-*p*-tolylpyridinato, M = Rh and Ir) by the chelating ligand 2,2′-biphenyldiamine (L_2) in a mixture of dichloromethane/methanol/water under reflux conditions. The intermediate formed chlorides $[M(ptpy)_2(L_2)]Cl$ yielded after metathesis with KPF_6 the corresponding hexafluoridophosphate salts (Eq. 1).

$$[\{M(\mu\text{-}Cl)(ptpy)_2\}_2] + 2\ bpda + 2\ KPF_6 \rightarrow 2\ [M(ptpy)_2(bpda)]PF_6 + 2\ KCl \quad (1)$$

(M = Rh, **1**; Ir, **2**; bpda = 2,2′-biphenyldiamine)

Both new compounds were obtained as yellow-orange crystals and characterized by elemental analysis, ^1H and $^{13}C\{^1H\}$ NMR spectroscopy, mass spectrometry, and by infrared as well as by UV-vis spectroscopy. Moreover, for **2** a single crystal X-ray diffraction study was undertaken. The ^1H and $^{13}C\{^1H\}$ NMR spectra of both new compounds confirmed the assumed molecular constitution. Furthermore, the ESI mass spectra

[a] M. Graf, Prof. Dr. H.-C. Böttcher, K. Sünkel
Department Chemie
Ludwig-Maximilians-Universität
Butenandtstrasse 5–13 (D)
81377 München, Germany
Fax: +49-89-2180-77407
E-mail: hans.boettcher@cup.uni-muenchen.de
[b] N. Metzler-Nolte, S. Thavalingam
Faculty for Chemistry and Biochemistry
Chair of Inorganic Chemistry – Bioinorganic Chemistry
Ruhr University Bochum
Universitätsstrasse 150
44801 Bochum, Germany
[c] R. Czerwieniec
Institute of Physical and Theoretical Chemistry
University Regensburg
Universitätstr. 31
93053 Regensburg, Germany

showed the molecular peaks for the mononuclear complexes (see Experimental Section).

Molecular Structure of Compound 2

Compound **2** crystallized from a mixture containing dichloromethane/methanol/*n*-heptane in the monoclinic space group $P2_1/n$ with one molecule in the asymmetric unit. As the examination of the dataset by the program PLATON showed the presence of 9.4% solvent accessible void volume, the SQUEEZE subroutine of PLATON was used for final refinements.[5] As expected the two cyclometalated 2-(*p*-tolyl)pyridinato ligands have the pyridine *N*-atoms in trans configuration. The 2,2′-biphenyldiamine ligand acts as a chelating *N,N*-donor to give a seven-membered puckered ring with a bite angle of ca. 88°. The phenyl rings of the 2,2′-biphenyldiamine (bpda) ligand are twisted by 66.33(14)°. Both amino functions are involved in N–H···F hydrogen bonds to the PF_6 anions, thus forming an infinite chain of alternating cations and anions along the *b* axis. Additional C–H···F hydrogen bonds link neighbouring chains in the *c* direction. As 2,2′-biphenyldiamine is a potential atropisomeric ligand,[6] and there are three chelating bidentate ligands at the iridium centre, four stereoisomers are possible: Δ(δ), Δ(λ), Λ(δ) and Λ(λ). However, as was also observed with the structurally related $[Co(bipy)_2(bpda)]^{3+}$ [Δ(δ)/ Λ(λ)][7] and $[Ru(bipy)_2(bpda)]^{2+}$ [Δ(δ)/ Λ(λ)][8] there is also in the case of **2** only the Δ(δ)/ Λ(λ) enantiomeric pair in the crystal. An ORTEP view of the molecular structure of cations in **2** is shown in Figure 1.

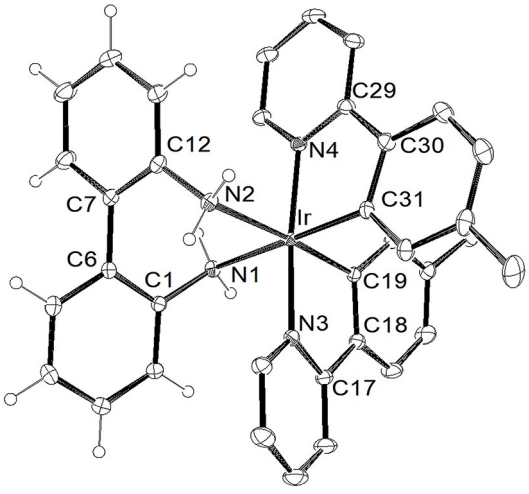

Figure 1. Molecular structure of the cation of **2** (only Λ(λ) enantiomer shown) in the crystal (ORTEP drawing and atom labeling scheme with 30% probability level). Selected bond lengths /Å and angles /°: Ir-N1, 2.228(2); Ir-N2, 2.245(2); Ir-N3, 2.051(2); Ir-N4, 2.053(2); Ir-C31, 1.998(2); Ir-C19, 2.002(3); N3-Ir-N1, 85.37(8); C19-Ir-N1, 88.73(8); C31-Ir-N1, 178.25(9); C19-Ir-N2, 176.05(8); N3-Ir-N4, 174.83(8).

Photophysical properties

UV/Vis-absorption spectra of compounds **1** and **2** were recorded in ethanol at ambient temperature. The spectra are shown in Figure 2.

In the short-wavelength region below 340 nm, a series of overlapping strong bands are present, at positions approximately the same for both complexes. For example, for rhodium complex **1**, apparent maxima are at 303 nm and 267 nm. The strong absorptions in this region are unequivocally due to π→π* excitations of the organic ligands ptpy and bpda. In the longer wavelength region, distinct MLCT (metal to ligand charge transfer) bands of lower intensity, peaking at 380 nm (**1**) and 392 nm and 418 nm (**2**) are present. The assignments are done in analogy with similar cyclometalated metal complexes[9] and are in accordance with results of TD-DFT calculations (see below).

Iridium complex **2** is luminescent at ambient temperature. The respective emission spectrum recorded in ethanol is shown in Figure 3. The partly resolved emission band is centred in the green spectral region at about 500 nm. The photoluminescence quantum yield ϕ_{PL} is within the margin of error of our quantum yield measurement system, which is ±2%; the decay time measured for a degassed sample is 1.2 µs (cf. Table 1). This relatively long decay time, in particular combined with the low ϕ_{PL} value, points to a spin forbidden character of the electronic transition. The emission is thus assigned to the lowest excited

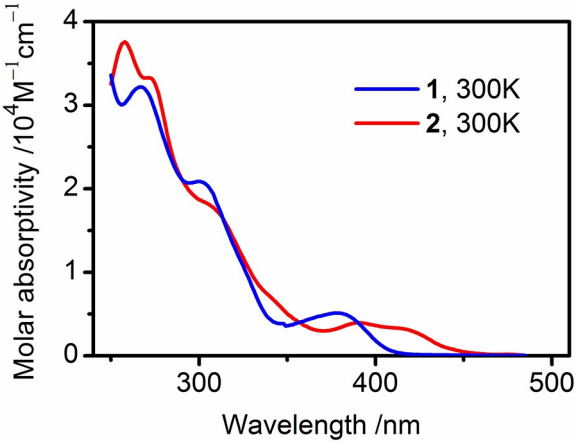

Figure 2. Ambient temperature UV/Vis absorption spectra of **1** and **2** in ethanol.

Table 1. Luminescence properties of **1** and **2** measured in ethanol at ambient temperature and at 77 K.

	Emission maximum λ_{em} *	Decay time τ
1 77 K	466 nm	130 µs
2 300 K	489 nm	1.2 µs
2 77 K	482 nm	4.7 µs

* highest energy maximum (0-0 vibronic transition)

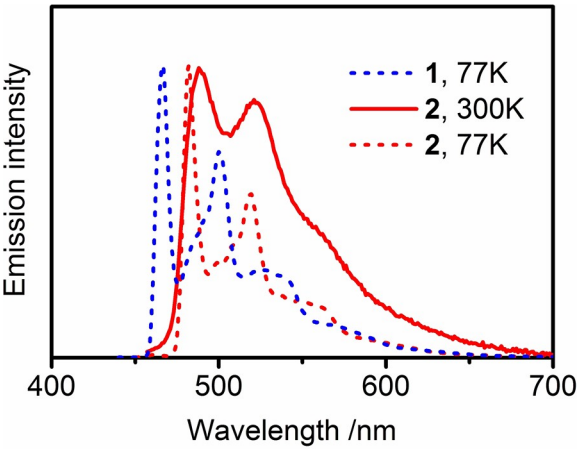

Figure 3. Photoluminescence spectra of complexes **1** (blue) and **2** (red) recorded in ethanol at ambient temperature (solid line) and at 77 K (dashed lines).

triplet state T_1 with mixed LC (ligand-centred; ptpy) and MLCT character (see below).

Upon cooling to 77 K, the emission band becomes sharper, revealing more details of the vibronic structure. The decay time becomes about four times longer according to less effective nonradiative relaxations to the ground state in a frozen rigid 77 K glass as compared to 300 K liquid. The 77 K emission spectrum of the rhodium congener **1** is essentially similar to that of **2**, with similar pattern of vibronic features. The band is shifted to a higher energy by about 700 cm^{-1} [λ_{em} shift from 482 nm (**2**, Ir) to 466 nm (**1**, Rh)] pointing to the essentially very similar origin of the emitting state. However, the decay time of the Rh complex **1** amounting to 130 μs is significantly longer than that of Ir complex to **2** due to different spin-orbit coupling constants of the two metals and differences in spin-orbit interactions of T_1 with higher singlet MLCT states.[10]

The origin of the electronic transitions of **1** and **2** was investigated by quantum chemical computations. Contour plots of selected molecular orbitals and orbital composition of the lowest-energy excited states are shown in Figure 4 and Table 2.

The highest occupied frontier orbitals (HOMO, HOMO-1, HOMO-2) of both complexes reveal high electron density in the toluene part of the cyclometalating ptpy ligands and different contributions of the metal. The lowest unoccupied orbitals (LUMO, LUMO+1, LUMO+2) are centered mainly at the pyridine parts of the ptpy ligands. The lowest-energy electronic transitions involve, thus, significant charge redistribution within the molecule from electron-rich fragments of ptpy and metal to electron-deficient parts of ptpy. In particular, these calculations fully support the assignment of the lowest excited triplet state T_1 as mixed ^{3}LC/MLCT state. However, owing to a close proximity of the calculated vertical transitions a precise assignment of the (relaxed) emitting state is difficult.

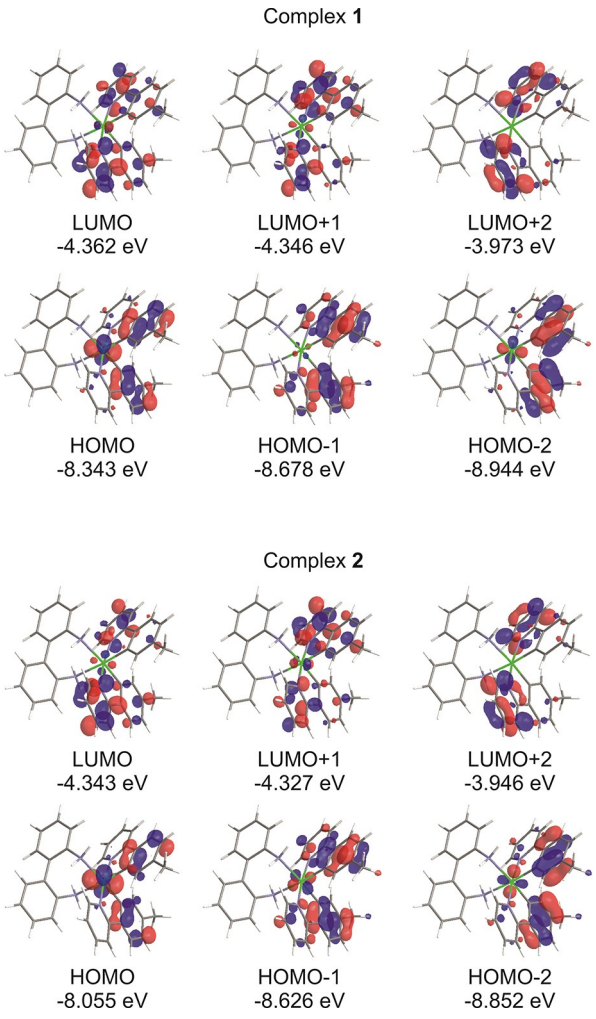

Figure 4. Contour plots of Kohn-Sham orbitals calculated for complexes **1** and **2** (isomers Λ) at the B3LYP/Def2-TZVP theory level.

Biological Activity of 1 and 2

To continue our investigations in the field of these promising class of complexes, the in vitro antiproliferative activity of the novel compounds **1** and **2** was evaluated by an MTT assay on the two malignant human cancer cell lines HT-29 (colorectal adenocarcinoma) and MCF-7 (breast adenocarcinoma). Recently we reported similar activity studies on two related compound bearing the 9,10-diaminophenanthrene (Ir) and the 9,10-diiminophenanthrene (Rh) ligand, respectively.[11] Both compounds were found to provide antiproliferative activity against both tested cell lines. A high activity was found for compounds **1** and **2** with IC_{50} values in the low micromolar range and an approximately tenfold increase in activity compared to cisplatin (see Table 3).

These IC_{50} values show especially against the cancer cell line HT-29 a remarkable increase in cytotoxicity compared to cisplatin for both, the rhodium and iridium complex. While the values of complex **1** corresponds to a nearly sixfold increase,

Table 2. Vertical excited state energies and orbital origins revealed by TD-DFT computations on complexes **1** and **2** in the ground state molecular geometry (isomers Λ) at the B3LYP/Def2-TZVP theory level.

Excitation	Energy /eV	One-electron contributions
Complex **1** (Rh)		
$S_0 \rightarrow S_1$	3.243	HOMO→LUMO (93%)
$S_0 \rightarrow T_1$	2.758	HOMO→LUMO (53%)
		HOMO-1→LUMO + 1 (26%)
$S_0 \rightarrow T_2$	2.767	HOMO→LUMO + 1 (48%)
		HOMO-1→LUMO (31%)
$S_0 \rightarrow T_3$	3.234	HOMO→LUMO + 1 (35%)
		HOMO-2→LUMO + 1 (13%)
		HOMO-1→LUMO (10%)
		HOMO-1→LUMO + 2 (9%)
Complex **2** (Ir)		
$S_0 \rightarrow S_1$	2.985	HOMO→LUMO + 1 (90%)
$S_0 \rightarrow T_1$	2.640	HOMO→LUMO + 1 (68%)
		HOMO-1→LUMO (17%)
$S_0 \rightarrow T_2$	2.652	HOMO→LUMO (67%)
		HOMO-1→LUMO (19%)
$S_0 \rightarrow T_3$	3.052	HOMO→LUMO (25%)
		HOMO-1→LUMO + 1 (24%)
		HOMO-2→LUMO (16%)
		HOMO-1→LUMO + 2 (7%)

Table 3. IC_{50} values in μM (by MTT assay) for **1** and **2** against MCF-7 and HT-29 cells. All data were measured in quadruplicates with 48 h incubation time. Cisplatin was used as a positive control, treated under identical conditions (with 0.5% final DMSO concentration in all cases).

	IC_{50} [μM] HT-29	IC_{50}[μM] MCF-7
1-Rh	5.7 ± 0.6	4.6 ± 0.6
2-Ir	11.4 ± 0.4	7.8 ± 0.4
cisplatin	38.3 ± 8.0	8.4 ± 0.9

the analogous iridium complex **2** shows an approximately threefold increase only in antiproliferative activity compared to cisplatin. A similar trend was also observed in the cytotoxic activity of compounds **1** and **2** in MCF-7 cells by comparison to cisplatin. While the Ir(III) species shows similar values as cisplatin around 10 μM, the Rh(III) species points out an approximately twofold decrease in its cytotoxicity. According to the obtained IC_{50} values the Rh(III) and Ir(III) complexes exhibit higher antiproliferative effects than cisplatin against the two cancer cell lines HT-29 and MCF-7. It is also noteworthy that the Rh(III) complex **1** shows an even higher impact on cancer cells than the Ir(III) complex, containing the same ligand system. These data lead us to the assumption that especially the activity of the Rh(III) complex seems to be more effective than cisplatin and the Ir(III) complex, which may result from different mechanisms of action or the formation of more stable DNA adducts. Further investigations on different Rh(III) complexes will show whether the low IC_{50} values originate solely from the physiochemical properties of the metal core, or if the enhanced IC_{50} values are due to the specific ligand system of 2,2′-biphenyldiamine.

Conclusions

The synthesis and the characterization of two new bis-cyclometalated compounds $[M(ptpy)_2(L_2)]PF_6$ (M = Rh, **1**; M = Ir, **2**) containing the chelating ancillary ligand L_2 = 2,2′-biphenyldiamine is reported. Characterization includes the confirmation of the molecular structure of **2** in the solid state by X-ray single-crystal structure determination. The iridium complex **2** is luminescent at ambient temperature. Its emission is associated with the lowest excited triplet state of the ^{3}LC/MLCT character localized at the molecular fragment $Ir(ptpy)_2$. Spectroscopically, with respect to the emission, the diamine ligand dpda acts as a spectator ligand. Moreover, the biological activities of compounds **1** and **2** were investigated. Both species exhibit cytotoxic effects towards two cell lines (HT29 and MCF-7) showing significant cytotoxicity with IC_{50} values in the low micromolar range, lower than those of cisplatin in all cases.

Experimental Section

General: All manipulations were performed under an atmosphere of dry nitrogen using conventional Schlenk techniques. Solvents were dried with standard procedures and stored under nitrogen. 2-(*p*-tolyl)pyridine and 2,2′-biphenyldiamine were purchased from Sigma-Aldrich and used as received. The starting complexes $[\{M(\mu\text{-}Cl)(ptpy)_2\}_2]$ (M = Rh, Ir) were prepared following literature methods.[12] NMR spectra were recorded using a Jeol Eclipse 400 instrument. Chemical shifts were referenced to the CD_2Cl_2 signal $\delta = 5.31$ ppm for ^{1}H and 53.8 ppm for $^{13}C\{^1H\}$ NMR spectra. IR spectra were recorded from KBr pellets with a Bruker FT/IR spectrometer (IFS 66) under an argon atmosphere. Mass spectra were obtained with a JeolMstation JMS 700 instrument. Elemental analyses (C, H, N) were performed by the Microanalytical Laboratory

of the Department of Chemistry, LMU Munich, using a Heraeus Elementar Vario EL instrument.

Photophysical measurements

UV-vis absorption spectra were measured using a Varian Cary 300 double-beam spectrometer with the sample held in a quartz cuvette of path length 1 cm. Spectra were recorded against a pure solvent in an optically matched cuvette. Emission spectra were measured with a Jobin Yvon Fluorolog-3 steady-state fluorescence spectrometer. Photoluminescence quantum yields were determined with a Hamamatsu C9920-02 system. The emission decay times were measured with a PicoBright PB-375 pulsed diode laser (λ_{exc} = 378 nm, pulse width 100 ps) as an excitation source was. The PL signal was detected with a cooled photomultiplier attached to a FAST ComTec multichannel scalar PCI card with a time resolution of 250 ps.

DFT and TD-DFT calculations

Quantum mechanical computations were carried out using the NWChem 6.6 computer program package.[13] The ground state molecular structure was optimized using the PBE0 functional and Def2-SVP atomic basis set for all atoms except Ir, for which Def2-TZVP basis set with appropriate effective core potentials obtained from the Basis Set Exchange repository[14] was used. For these ground state geometries 20 singlet and triplet excitations were calculated using the same functional and atomic basis sets, respectively. The calculations were done for both Λ and Δ isomers of each compound resulting in the same orbital and excited state energies.

Biological activities

Dulbecco's Modified Eagle's Medium (DMEM), containing 10% fetal calf serum, 1% penicillin and streptomycin, was used as growth medium. MCF-7 and HT-29 cells were detached from the wells with trypsin and EDTA, harvested by centrifugation and resuspended again in the cell culture medium. The assays were carried out on 96 well plates with 6000 cells per well for MCF-7 and HT-29. After 24 h of incubation at 37 °C and 10% CO_2, the cells were treated with the compounds **1** and **2** (with DMSO concentrations of 0.5%) with a final volume of 200 µl per well. For a negative control, one series of cells was left untreated. The cells were incubated for 48 h followed by adding 50 µl MTT (2.5 mg/ml). After an incubation time of 2 h, the medium was removed and 200 µl DMSO were added. The formazan crystals were dissolved, and the absorption was measured at 550 nm, using a reference wavelength of 620 nm. Each test was repeated in quadruplicates in three independent experiments for each cell line.

Synthesis of 1 and 2: To a solution of [{M(µ-Cl)(ptpy)$_2$}$_2$] (M = Rh, Ir) (0.15 mmol) in 25 mL of a mixture of CH_2Cl_2/MeOH/H_2O (1:1:0.5) the ligand 2,2′-biphenyldiamine (0.3 mmol) was added and the mixture refluxed with stirring for 2 h. After cooling to room temperature, KPF_6 (0.5 mmol) was added and the solution stirred for additional 20 minutes. The solvent was removed to dryness in vacuo and the residue dissolved in dichloromethane and chromatographed on alumina with CH_2Cl_2/acetone (9:1) as the eluent. The resulting solution was evaporated to dryness and the residue was re-dissolved in 5 ml of dichloromethane and the product was precipitated by slow diffusion of MeOH/*n*-heptane.

[Rh(ptpy)$_2$(2,2′-biphenyldiamine)]PF$_6$ (1) Yield: 120 mg (52.1%). *Anal.* Calc. for $C_{36}H_{32}F_6N_4PRh$ (768.55): C, 56.26; H, 4.20; N, 7.29. Found: C, 56.18; H, 4.50; N, 7.06%. MS (FAB$^+$): *m/z* = 623.16 [M$^+$] complex cation. **^{1}H NMR** (400 MHz, CD_3OD): δ = 7.97 (m, 4H), 8.02 (m, 2H), 7.64 (d, *J* = 8 Hz, 2H), 7.54 (d, *J* = 6 Hz, 2H), 7.23 (m, 2H), 7.05 (m, 2H), 6.94 (dt, *J* = 1.6 Hz, *J* = 7.4 Hz, 2H), 6.86 (d, *J* = 8 Hz, 2H), 5.9 (s, 2H), 5.86 (d, *J* = 8 Hz, 2H), 4.30 (d, *J* = 10 Hz, 2H, NH_2), 3.90 (d, *J* = 10 Hz, 2H, NH_2), 2.0 (s, 6H). **^{13}C {^{1}H} NMR** (100 MHz, CD_2Cl_2): δ = 164.8, 163.3 (Rh–C, *J* = 34.4 Hz), 148.4, 144.3, 140.7, 140.6, 139.7, 138.6, 134.4, 131.4, 129.5, 128.1, 125.5, 125.0, 123.0, 119.7, 118.6, 21.5. **IR** (KBr, cm^{-1}): 3349 m, br; 3298 m, br; 3030 m, br, sh; 2955 m, br; 2917 m, br; 2866 m, br; 1606 s, 1586 s, 1565 m, 1504 m, 1482 s, 1465 m, 1447 m, 1429 m, 1377 m, br; 1317w, 1304w, 1270w, 1241w, 1213w, 1162w, 1061 m, sh; 1030 m, 1008 m, sh; 843vs, br; 771 s, sh; 751 s, sh; 720w, 676w, 557 s, 500w, 490w, 450w, 427w. **UV/vis** 0.05 mM, CH_2Cl_2 (nm): 243 (42.600), 270 (33.200), 302 (20.400), 378 (5940), 414 (580).

[Ir(ptpy)$_2$(2,2′-biphenyldiamine)]PF$_6$ (2) Yield: 140 mg (54.4%). *Anal.* Calc. for $C_{36}H_{32}F_6IrN_4P$ (857.86): C, 50.40; H, 3.76; N, 6.53. Found: C, 50.73; H, 3.83; N, 6.19%. MS (FAB$^+$): *m/z* = 713.22 [M$^+$] complex cation. **^{1}H NMR** (400 MHz, CD_3OD): δ = 7.97 (d, *J* = 7.6 Hz, 2H), 7.86 (dt, *J* = 1.6 Hz, *J* = 7.4 Hz, 2H), 7.60 (m, 4H), 7.24 (m, 4H), 6.99 (m, 4H), 6.80 (dd, *J* = 0.8 Hz, *J* = 8.0 Hz, 2H), 6.00 (s, 2H), 5.86 (d, *J* = 7.6 Hz, 2H), 4.76 (d, *J* = 10.8 Hz, 2H, NH_2), 4.06 (d, *J* = 11.2 Hz, 2H, NH_2), 2.06 (s, 6H). **^{13}C {^{1}H} NMR** (100 MHz, CD_2Cl_2): δ = 167.9, 148.2, 144.6, 141.0, 140.7, 138.7, 138.4, 133.6, 131.7, 129.5, 128.4, 126.1, 124.8, 124.0, 122.9, 119.4, 118.7, 21.5. **IR** (KBr, cm^{-1}): 3333 m, br; 3283 m, br; 3029 m,br, sh; 2957 m, br; 2919 m, br; 2861 m, br; 1607 s, 1588 s; 1564 m, 1504 m, 1478 s, 1465 m, 1447 m, 1429 m, 1388 m; 1317w, 1305w, 1268w, 1240w, 1211w, 1162w, 1101 m, br, sh; 1035 m, 1008w, 843vs, br; 768 m, br; 751 m, br, sh; 720w, 678w, 557 s, 505w, 493w, 450w, 427w. **UV/vis** 0.05 mM, CH_2Cl_2 (nm): 258 (31.500), 273 (28.000), 309(14.750), 392 (1720) 418 (1150).

Table 4. Experimental details of the crystal structure determination of **2**.

Compound	**2**
Empirical formula	$C_{36}H_{32}F_6IrN_4P$
Formula weight	857.82
Temperature /K	150 (2)
Crystal system	monoclinic
Space group	$P2_1/n$
Unit cell dimensions	
a/Å	9.8866(2)
b/Å	20.7453(5)
c/Å	17.0501(4)
β/°	101.4850(10)
Volume /Å^3	3426.96(14)
Z	4.007
ρ calcd./g·cm^{-3}	1.663
μ /mm^{-1}	4.007
θ range/°	2.628–30.536
Reflections, collected	62426
Reflections, independent	10478
R_{int}	0.0331
wR_2 (all data)	0.0621
R_1	0.0216
S	1.099
$\Delta\rho_{fin}$ (max/min)/e·Å^{-3}	0.823/−0.880

X-ray Structural Determination: Crystals of **2** suitable for X-ray diffraction were obtained by crystallization from mixtures of dichloromethane/methanol/*n*-heptane at ambient temperature. Crystals were selected by means of a polarization microscope, mounted on a MiTeGen MicroLoop, and investigated with a Bruker D8 Venture TXS diffractometer using Mo-Kα radiation (λ =

0.71073 Å). The structure was solved by direct methods (SHELXT)[15] and refined by full-matrix least-squares calculations on F^2 (SHELXL-2014/7)[16] as implemented in the WINGX structure package.[5] Anisotropic displacement parameters were refined for all non-hydrogen atoms. Details of the crystal data, data collection, structure solution, and refinement parameters of compound **2** are summarized in Table 4.

Crystallographic data (excluding structure factors) for the structure in this paper have been deposited with the Cambridge Crystallographic Data Centre, CCDC, 12 Union Road, Cambridge CB21EZ, UK. Copies of the data can be obtained free of charge upon quoting the depository number CCDC-1949667 (**2**) (Fax: +44-1223-336-033; E-Mail: deposit@ccdc.cam.ac.uk, http://www.ccdc.cam.ac.uk).

Acknowledgements

The authors are grateful to the Department of Chemistry of the Ludwig Maximilians Universität Munich for financial support. *P. Mayer* is acknowledged for collecting the X-ray crystal data. RC acknowledges the Deutsche Forschungsgemeinschaft (DFG) for support. Open access funding enabled and organized by Projekt DEAL.

Keywords: 2,2′-Biphenyldiamine · Cyclometalated complexes · Cytotoxic activity · Iridium · Rhodium

[1] a) K. J. Franz, N. Metzler-Nolte, *Chem. Rev.* **2019**, *119*, 727; b) E. Alessio (Ed.), *Bioinorganic Medicinal Chemistry*, Wiley-VCh, Weinheim, **2011**; c) G. Gasser, N. Metzler-Nolte, *Curr. Opin. Chem. Biol.* **2012**, *16*, 84; d) G. Gasser, I. Ott, N. Metzler-Nolte, *J. Med. Chem.* **2011**, *54*, 3.

[2] a) A. Zamora, G. Vigueras, V. Rodríguez, M. D. Santana, J. Ruiz, *Coord. Chem. Rev.* **2018**, *360*, 34; b) L. He, K.-N. Wang, Y. Zheng, J.-J. Cao, M.-F. Zhang, C.-P. Tan, L.-N. Ji, Z.-W. Mao, *Dalton Trans.* **2018**, *47*, 6942.

[3] P. Laha, U. De, F. Chandra, N. Dehury, S. Khullar, H. S. Kim, S. Patra, *Dalton Trans.* **2018**, *47*, 15873.

[4] M. Graf, D. Siegmund, Y. Gothe, N. Metzler-Nolte, K. Sünkel, *Z. Anorg. Allg. Chem.* **2020**, *646*, 665 and references cited therein.

[5] a) WINGX: L. J. Farrugia, *J. Appl. Crystallogr.* **1999**, *32*, 837; b) PLATON: A. L. Spek, *J. Appl. Crystallogr.* **2003**, *36*, 7.

[6] S. S. Alguindigue, M. A. Khan, M. T. Ashby, *Organometallics* **1999**, *18*, 5112.

[7] T. Tanamura, H. Ito, J. Fujita, K. Saito, S. Hirai, K. Yamasaki, *J. Coord. Chem.* **1973**, *3*, 161.

[8] S. S. Alguindigue, M. A. Khan, M. T. Ashby, *Inorg. Chim. Acta* **2000**, *310*, 156.

[9] a) J. C. DEATON, F. N. CASTELLANO, "Archetypal Iridium(III) Compounds for Optoelectronic and Photonic Applications in E. Zysman-Colman (ed.) Iridium (III) in optoelectronic and photonics applications, Wiley-VCH, Weinheim, **2017**, pp. 1–69; b) H. Yersin, A. F. Rausch, R. Czerwieniec, T. Hofbeck, T. Fischer, *J. Coord. Chem.* **2011**, *255*, 2622.

[10] M. Z. Shafikov, R. Daniels, V. N. Kozhevnikov, *J. Chem. Phys. Lett.* **2019**, *10*, 7015.

[11] M. Graf, D. Siegmund, N. Metzler-Nolte, K. Sünkel, *Z. Anorg. Allg. Chem.* **2019**, *645*, 1068.

[12] a) H.-C. Böttcher, M. Graf, K. Sünkel, P. Mayer, H. Krüger, *Inorg. Chim. Acta* **2011**, *365*, 103; b) K. Sünkel, M. Graf, H.-C. Böttcher, B. Salert, H. Krüger, *Inorg. Chem. Commun.* **2011**, *14*, 539.

[13] M. Valiev, E. J. Bylaska, N. Govind, K. Kowalski, T. P. Straatsma, H. J. J. van Dam, D. Wang, J. Nieplocha, E. Apra, T. L. Windus, W. A. de Jong, *Comput. Phys. Commun.* **2010**, *181*, 1477.

[14] B. P. Pritchard, D. Altarawy, B. Didier, T. D. Gibson, T. L. Windus, *J. Chem. Inf. Model.* **2019**, *59*, 4814.

[15] G. M. Sheldrick, *Acta Crystallogr. Sect. A* **2015**, *71*, 3.

[16] G. M. Sheldrick, *Acta Crystallogr. Sect. C* **2015**, *71*, 3.

Manuscript received: December 14, 2020
Revised manuscript received: January 25, 2021

